How Far is Too Far? The Trade-Off between Selection Distance and Accuracy during Teleportation in Immersive Virtual Reality

Daniel Rupp O, Tim Weissker O, Matthias Wölwer O, Torsten W. Kuhlen O, Daniel Zielasko

Abstract—Target-selection-based teleportation is one of the most widely used and researched travel techniques in immersive virtual environments, requiring the user to specify a target location with a selection ray before being transported there. This work explores the influence of the maximum reach of the parabolic selection ray, modeled by different emission velocities of the projectile motion equation, and compares the resulting teleportation performance to a straight ray as the baseline. In a user study with 60 participants, we asked participants to teleport as far as possible while still remaining within accuracy constraints to understand how the theoretical implications of the projectile motion equation apply to a realistic VR use case. We found that a projectile emission velocity of $14\frac{m}{s}$ (resulting in a maximal reach of 21.52 m) offered the best trade-off between selection distance and accuracy, with an inferior performance of the straight ray. Our results demonstrate the necessity to carefully set and report the projectile emission velocity in future work, as it was shown to directly influence user-selected distance, selection errors, and controller height during selection.

Index Terms—Virtual Reality, Navigation, Teleportation, Target Selection, Fitts' Law.

1 Introduction

VIRTUAL reality (VR) technology has become more widely adopted in recent years, and the complexity of developing VR applications has decreased as most game engines support VR devices and provide default implementations for fundamental features like navigation. Target-selection-based teleportation or point-and-click teleportation (often referred to as *teleportation* for brevity) has emerged as a standard for navigation in virtual environments, allowing users to egocentrically select a target location before being automatically repositioned there [42]. Due to the relocation being instantaneous, teleportation is more efficient than continuous methods, especially when traversing large distances [12], [44]. Furthermore, various studies have shown that teleportation-based travel techniques prevent cybersickness as these techniques avoid

Daniel Rupp, Tim Weissker, and Torsten W. Kuhlen are with the Visual Computing Institute at RWTH Aachen University. E-mail: daniel.rupp@rwth-aachen.de, me@tim-weissker.de, kuhlen@vr.rwth-aachen.de.

Matthias Wölwer is with the Human-Computer Interaction Group at Trier University. E-mail: woelwerm@uni-trier.de.

Daniel Zielasko is with the Technical University of Denmark, Denmark. Email: daniel.zielasko@rwth-aachen.de.

contradictory visual cues of self-motion that can lead to discomfort and are, therefore, often preferred over continuous techniques [9], [12], [42]–[44], [57].

Teleportation is one of the most researched travel techniques [38]. Multiple researchers have evaluated central factors like spatial awareness [2], [5], [11], [31], [33], [41], performance [4], [7], [12], [17], [18], [27], [33], adapted teleportation to other degrees of freedom [45], [54], [55], or changed their parametrization [19], [58]. A key component of teleportation-based navigation techniques is the selection mechanism to specify the target location, which often involves the use of parabolic arcs [42]. These can be computed using the projectile motion equation, which traces an imagined projectile emitted from the controller as it falls down to the ground due to gravity. The projectile's intersection point with the scene's geometry then determines the target location.

One parameter that is of particular relevance for teleportation is the initial velocity at which the simulated projectile is emitted from the user's controller, as it directly affects the maximal distance at which target locations can be selected. While the ability to select targets further away potentially increases navigation efficiency, this likely comes at the cost of reduced selection accuracy as far-away targets become more difficult to see. Although this trade-off is central to the informed choice of teleportation parameters for a given navigation task, it has not yet been examined empirically, and no best practice recommendations exist up to date. What is more, most research papers in the field do not report on their parameter selection for teleportation, making comparisons across publications challenging [60].

To provide scientific insights on the appropriate choice of selection parameters for teleportation, this paper addresses the following research question:

RQ: How does the maximal reach of the teleport parabola affect the trade-off between selection distance and accuracy?

To answer this question, we provide theoretical results by looking at the mathematical background of the target selection process as well as empirical results from a withinsubjects user study with 60 participants. In the study, participants had to find a balance between far and accurate teleports. Users were told to teleport as far as possible but

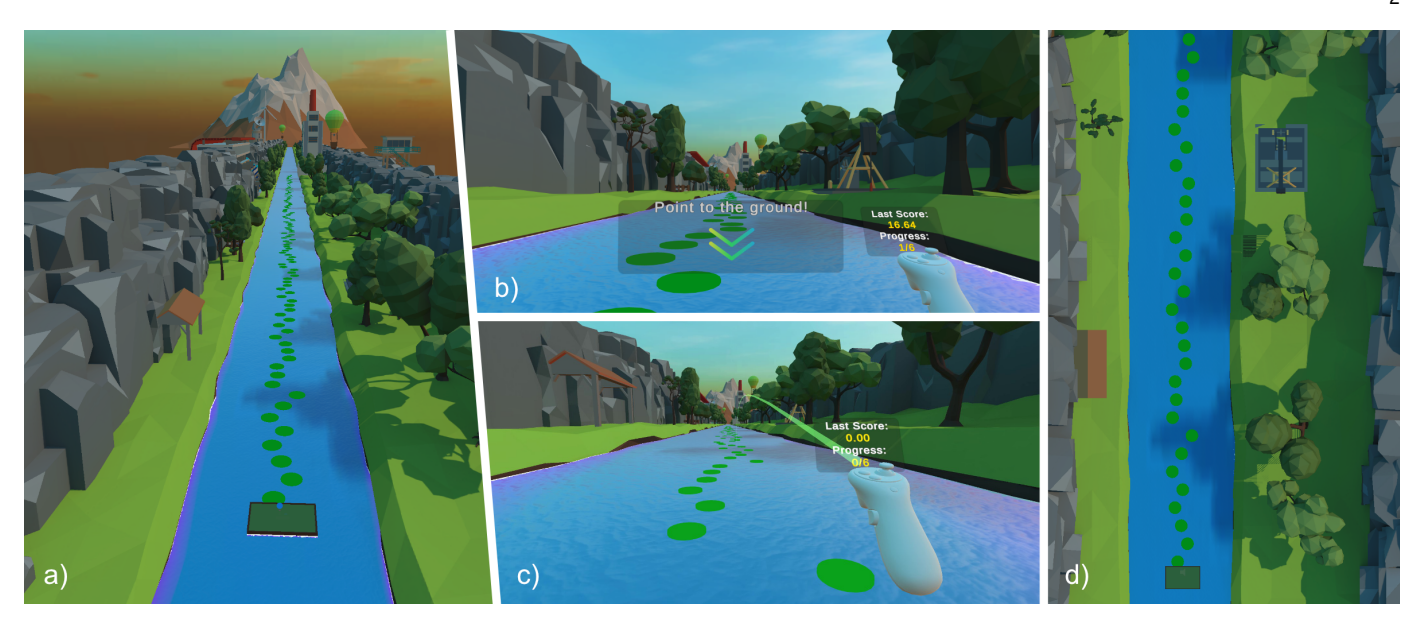


Fig. 1. Overview of the environment used during our user study. Participants were positioned on a longitudinal river (a) starting at a rectangular starting area, with various circular platforms in the form of water lilies spawned in front of them (d). Before being able to teleport onto a platform, users were prompted to point the controller to the ground (b), so the target selection process was initiated from a defined starting point. Afterward, users could choose a target platform by aiming with the controller so that the parabolic arc intersects with a platform (c). A textbox was attached to the controller, showing a score based on the selected distance and the remaining number of teleports in the current task.

still be able to hit a target platform accurately. We then analyzed how different values for the projectile's initial velocity, which directly affects the maximal reach, influence the chosen teleportation distance and accuracy. We conducted our study under controlled conditions to isolate the influence of the projectile arc velocity, which is crucial to gain scientific insights and establish causal relationships before introducing additional (and potentially confounding) variables in a more ecologically valid, real-world usage scenario.

In summary, our work led to the following contributions:

- a detailed derivation of the mathematical background of the target selection process of targetselection-based teleportation,
- the derivation of a novel performance measurement for teleportation techniques similar to the throughput value of Fitts' Law,
- scientific evidence from a user study with 60 participants analyzing the influence of the maximal reach on the selected teleportation distance and accuracy comparing ten target selection strategies (nine parabolic arcs with different velocities and a straight ray), showing that there is a velocity threshold at $14\frac{m}{s}$ beyond which accurately selecting a target platform becomes less feasible.

The analysis in our controlled scenario underlines the importance of the appropriate parametrization of teleportation-based navigation. They highlight that application designers should not indefinitely increase the projectile velocity and, therefore, the maximum reach of the selection parabola, as targets will become increasingly challenging to select accurately.

2 RELATED WORK

Our work is based on prior research about teleportationbased navigation in virtual environments. In Section 2.1, we will first explore general research about target-selectionbased navigation and focus more explicitly on the target selection process in Section 2.2.

2.1 Target-Selection-Based Teleportation

Target-selection-based teleportation, often simply referred to as teleportation or point & teleport [6], has emerged as a standard for VR locomotion. In a literature review by Martinez et al. about research trends for VR locomotion [38], teleportation was the highest-researched technique.

In the classification of travel metaphors presented by LaViola et al., teleportation falls under the category of selection-based travel metaphors [34], where users select a target location from an egocentric perspective. The selection is usually made via a tracked device from which a ray is cast into the environment [6], [42]. The intersection point of that ray with the geometry in the scene then determines the target location. The target location can be confirmed with a trigger, and the user's viewpoint instantly transitions to the selected location.

To formalize this more generally, Weissker et al. provided a classification for target-based travel techniques [57]. They suggest that teleportation, amongst others, can be broken down into four sequential steps. 1) target specification: the user specifies a target location based on some form of selection mechanism, 2) pre-travel information: the user receives visual assistance to specify the target location or to comprehend the forthcoming transition, 3) transition: the user transitions to the specified target location either instantly or in a speed-up motion potentially with a fade-to-black animation, and 4) the optional post-travel feedback.

To get an overview of different teleportation techniques, Prithul et al. conducted a mini-review about teleportation [42]. They included papers that featured an empirical evaluation using head-mounted displays. Starting from two popular sources from Bozgeyikli et al. [6] and Bowman et al. [5], articles were selected according to these criteria. In the end, 27 papers were taken into account. The papers were clustered into either 1) comparative studies between teleportation and other navigation techniques, and 2) advancements to teleportation. Results across publications showed that teleportation causes almost no cybersickness and improves performance but reduces presence and increases spatial disorientation.

In earlier papers, the target location is often specified via a straight ray. In recent years, parabolic arcs have been used more often due to their ability to teleport on top of elevated terrain or over obstacles. Out of the 27 papers considered by Prithul et al. [42] in their mini-review about teleportation, seven papers used a straight ray [6], [7], [11], [18], [31], [37], [41], while 13 used a parabolic arc [4], [12], [14], [15], [17], [25]–[27], [33], [35], [36], [53], [56]. The remaining papers used either a direct form of target specification or did not rely on a tracked controller.

In this paper, we will explore target-selection-based teleportation and look more closely at the target specification step, where users select a target location using a parabolic arc with various velocities or a straight ray, which is essentially a parabolic arc with infinite projectile velocity.

2.2 Target Specification

While the target specification step is fundamental to teleportation, implementation details are often inadequately specified. For example, Zielasko and Weissker analyzed 61 papers derived from a systematic review about navigation in VR and identified multiple problems regarding their reproducibility [60]. For teleportation-based techniques, the authors identified that the target specification process should mention the shape of the selection tool and the object to which it was attached. In case the selection tool is not a straight ray, parameters describing the appearance and maximum reach should be provided. Of the 27 teleport papers they analyzed, only 5 reported the maximal reach. In addition, in the mini-review from Prithul et al., [42], only one paper [27] out of the thirteen that used a parabolic arc specified the velocity of the projectile used to visualize the arc, while four said that they used the default implementation of the Steam VR plugin for Unity [12], [17], [26] or Unreal [4].

In the following sections, we will look at papers that report implementation details about the target specification distance in Section 2.2.1 and accuracy in Section 2.2.2. If papers mentioned the initial velocity of the parabolic arc, we calculated the maximal reach based on Equation 8, which we will cover in more detail in Section 3.

2.2.1 Target Specification Distance

Griffin et al. compared four navigation techniques, two "handsbusy" (steering via the trackpad and teleportation) and two "handsfree" (head tilt and walking in place) techniques in a large indoor environment [27]. For teleportation,

the authors used a parabolic arc with a velocity of $6 \, \frac{m}{s}$. Based on the given velocity, we computed the maximal teleportation distance to be around $5.07 \, m$. The value was chosen based on the walking-in-place method, so it is equal for all navigation techniques that they compared.

Freitag et al. developed an interactive system that aids users in the exploration of unknown indoor environments (university, dungeon, office) by suggesting unvisited points of interest [23]. In addition, users were able to freely explore the environments using teleportation. The authors specified that the teleport parabola had a maximal range of $7\ m$ but did not provide additional reasoning for that.

Badr and De Amicis developed three advancements of teleportation by adding: 1) a Mini-Map showing a top-down view of the user's surroundings, 2) a Portal Preview showing a preview of the target location, and 3) a X-Ray Vision that makes buildings transparent and lets users teleport to potentially obscured locations [48]. The user study had five conditions: a baseline condition with only teleportation, three conditions where one of the advancements was added, and a fifth condition with all advancements present. In all conditions, a parabolic arc with a maximal distance of up to 118 m was used to specify the target location. The authors did not provide any further details as to why this value was chosen. In the baseline condition, users teleported an average distance of about 3,901.84 m spread over 129.08 average teleports. This would result in an average distance per teleport of 30.23 m.

Simeone et al. developed a navigation technique called "SpaceBender" that "bends" the environment to prevent users from leaving the tracking space [49]. Their technique was compared to a redirection technique called "Stop and Reset" (based on Cools et al. [16]) as well as teleportation. Users were tasked to traverse a $100\ m$ long linear corridor. The parabolic arc in the teleport condition had a maximal range of $10\ m$.

Ke et al. compared a novel locomotion in place technique to teleportation [30]. The movement speed of their walking-in-place technique was calculated as "HeightOfUser/0.45" [30]. They also tested different factors of the walking speed up to a factor of 10. The maximal range of the parabolic arc used for teleportation was set to be equal to the maximal speed of the walking-in-place method. Together with the average user height of $172.3\ cm$ that they reported in their user study, we were able to calculate that they set the maximal range of the teleport to $38.3\ m$.

Weissker et al. compared the effects of teleportation and steering on spatial updating and simulator sickness [57]. Participants had to teleport a path of $300\ m$ divided by three path segments in an outdoor city environment. The distance of the parabolic arc was set to $180\ m$, so it was possible to cover a path segment in a single jump and potentially provoke spatial disorientation to measure differences between steering and teleportation.

Bhandari et al. developed a teleporting technique called *Dash* that uses a fast but continuous transition so users perceive some optical flow but not too much to induce cybersickness. In their study design, users had to teleport along different waypoints, which were positioned five to eleven meters apart as "selecting a waypoint that was more than 13 meters away was difficult" [3]. Based on the max-

Feld et al. analyzed different transition effects for pointing-based teleportation and their effects on cybersickness in a minimalistic and detailed environment [19]. In their study design, users had to teleport along a $300\ m$ long path. The maximum teleport distance was set to $15\ m$, requiring users to teleport more often to experience the transition effect they analyzed.

Paris et al. looked at path integration and compared two continuous techniques to two discrete ones in an outdoor environment [41]. In the teleport condition, the authors used a straight ray with a length of $20\ m$ to specify the target location. However, no reason was provided for this restriction.

Many papers report that they used the SteamVR plugin for Unreal or Unity [4], [12], [17], [26], which uses a value of $10 \ \frac{m}{s}$ resulting in a maximal teleport distance of around $11.69 \ m$. Newer implementations might rely on the default implementation of game engines, e.g., the XR Interaction toolkit from Unity has a maximal teleportation distance of around $10 \ m$ while the VR template of Unreal uses a value of $6.5 \ \frac{m}{s}$, which would result in a maximal teleportation distance of around $5.73 \ m$. The presented papers illustrate that the selected maximum distance differs vastly across publications (from $5.07 \ m$ to $180.00 \ m$ with a median of $11.68 \ m$), which motivates a more thorough empirical comparison of different parametrizations.

2.2.2 Target Specification Accuracy

Accuracy is an essential factor during travel and often in contrast to efficiency. During steering, for example, the steering law states that users have to reduce their speed when the movement requires more accuracy [59]. As the target specification step during teleportation is a type of selection task, a similar effect can be expected. However, this effect has not yet been analyzed and quantified in the context of teleportation.

First work in this direction has been done by Sindhupathiraja et al. [50]. They compared uni-manual with bi-manual hand-based teleportation and the influence of the user's posture. To compare the different teleport variations, they propose a modified version of Fitts' Law—a mathematical model to predict selection time based on the distance and width of the target—to measure and compare the teleport performance and accuracy. The focus of their evaluation, however, was not on the target specification but rather on the target confirmation step. The target confirmation was either done by a gesture using the aiming hand or the free hand or by using dwell time. The targets were position at $3\ m$ and $9\ m$ laterally and $\pm 3\ m$ vertically. Targets had a fixed width of either $0.2\ m$ or $1.35\ m$.

- 1. SteamVR plugin for Unreal
- 2. SteamVR plugin for Unity
- 3. XR Interaction Toolkit
- 4. Unreal VR Template

To our knowledge, no further research about selection accuracy in the specific context of teleportation, especially with parabolic selection rays, exists. Sindhupathiraja et al. [50] showed that Fitts' Law can be applied to teleportation in VR.

2.3 Summary

While most implementations presented in this section use a parabolic arc to specify the target location, the range of that arc varies drastically. The motivation behind the maximal teleportation distance is mainly influenced by the user study design to be comparable to other conditions tested or to be suitable for the specific environment at hand. It is, therefore, difficult to conclude general guidelines for implementing teleportation techniques that are generally applicable. For steering, the steering law suggests that there is a trade-off between speed and accuracy. However, this has not been analyzed yet in a teleportation context. This research gap further motivates our pursuit of testing the maximal reach of the teleport parabola and the influence on the selected teleport distance and accuracy. Fitts' Law, a model to analyze selection performance, might be a valuable tool for analyzing the target selection process of teleportation.

3 MATHEMATICAL BACKGROUND OF PARABOLIC TARGET SELECTION

In this section, we examine the mathematical background of the target selection process and highlight initial theoretical findings that form the basis of the hypotheses as well as the evaluation procedure of our user study. First, we look at the projectile motion equation and the influence of the selection distance and the initial pointing angle on accuracy. We then look at a modification of Fitts' Law's throughput value that allows us to compare different parametrizations of the teleport parabola.

3.1 Projectile Motion Equation

A prominent way of computing parabolic arcs that are used for the target selection process is to trace a projectile following the projectile motion equation in the forward direction of the controller. The point where the projectile intersects with the scene's geometry then determines the target location. The line the projectile follows is constantly visualized and updated according to the controller's position. The coordinate system we refer to and the parameters influencing the projectile can be seen in Figure 2. This parabolic arc is influenced by the controller's position (x_0,y_0) , the angle of the controller γ , the initial velocity of the projectile v_0 , and the gravity g.

The projectile's position (x: forward direction, y: up direction) is given at a certain point in time t via the following equation:

$$x = x_0 + v_x t y = y_0 + v_y t - \frac{1}{2} g t^2$$
 (1)

where (x_0, y_0) corresponds to the initial position of the projectile given by the position of the controller. Based on the controller's pointing angle γ , the initial projectile velocity

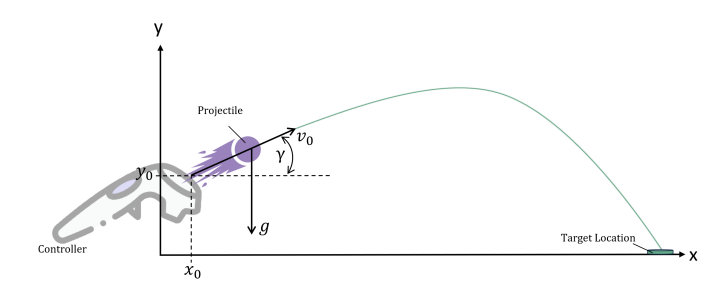


Fig. 2. The projectile arc is determined by the position (x_0,y_0) and angle γ of the controller, the initial velocity of the projectile v_0 , and the gravity a.

 v_0 is given in the forward direction of the controller. We can bring it into the formula using $v_x = v_0 \cos(\gamma)$ and $v_y = v_0 \sin(\gamma)$ to get the following equations:

$$x = x_0 + v_0 \cos(\gamma)t \tag{2}$$

$$y = y_0 + v_0 \sin(\gamma)t - \frac{1}{2}gt^2$$
 (3)

To calculate the distance given a velocity, we can use Equation 2, which only has t as an unknown parameter. After rearranging Equation 3 to t, we can substitute t in Equation 2 and get the following equation to calculate the travel distance of the projectile:

$$\frac{d(v_0, x_0, y_0) =}{x_0 + v_0 \cos(\gamma) \left(v_0 \sin(\gamma) + \sqrt{(v_0 \sin(\gamma))^2 - 2g(-y_0 + y)} \right)}{g}$$
(4)

3.1.1 Maximal Teleportation Distance

To get the maximal distance possible with a given velocity, we first calculate the optimal angle to reach the maximal distance. Contrary to intuition, the optimal pointing angle is not precisely at 45° as the starting point of our projectile is not on the ground level but at the user's hand $(y_0 > 0)$. To derive the formula for the optimal angle, we can start with Equation 4, which we can further simplify using the assumption that the projectile starts at $x_0 = 0$ and finishes at the ground level (y = 0) to get the following equation:

$$d(v_0, y_0) = \frac{v_0 \cos(\gamma) \left(v_0 \sin(\gamma) + \sqrt{(v_0 \sin(\gamma))^2 + 2y_0 g} \right)}{g}$$
(5)

We can now create the derivative of the previous formula with respect to γ and set it to zero to find the extreme points:

$$\frac{\partial d(v_0, y_0)}{\partial \gamma} = \frac{v_0^2 \cos^2(\gamma) \left(1 + \frac{v_0 \sin(\gamma)}{\sqrt{2gy_0 + v_0^2 \sin^2(\gamma)}}\right)}{g} - \frac{v_0 \sin(\gamma) \left(v_0 \sin(c) + \sqrt{2gy_0 + v_0^2 \sin^2(\gamma)}\right)}{g} = 0$$

$$= 0$$
(6)

If we now solve for γ , we get the following equation to calculate the optimal angle at which the projectile reaches the maximal distance.

$$\gamma_{opt}(v_0, y_0) = \cos^{-1}\left(\frac{\sqrt{v_0^2 + 2gy_0}}{\sqrt{2v_0^2 + 2gy_0}}\right) \tag{7}$$

If we now insert the optimal angle back into Equation 4, we have an equation to calculate the maximal possible teleportation distance for a given velocity:

$$\frac{d_{\max}(v_0, x_0, y_0) =}{x_0 + v_0 \cos(\gamma_{\text{opt}}) \left(v_0 \sin(\gamma_{\text{opt}}) + \sqrt{(v_0 \sin(\gamma_{\text{opt}}))^2 + 2y_0 g}\right)}{g}$$
(8)

3.1.2 Angle-Distance Relationship

To understand the connection between the previous formulas, we plotted the relationship between γ and the teleportation distance d, which can be seen in Figure 3. The plot was constructed for the exemplary velocity of $10 \frac{m}{s}$ and a straight ray at a controller height of 1.3 m. Note that for increasing velocities, the maximal teleport distance of the arc moves further to the left (towards 0°) and increases, therefore getting closer to the shape of the straight ray. The straight ray is essentially a parabolic arc with infinite velocity. From the plot in Figure 3, we can see that the angle-distance relationship is not linear. For example, when we look at the arc in case the user moves the controller from 0° to 20° , the target location moves by about 4 m, while between 30° and 50° , the target location moves by less than 1 m. The curve's steepness correlates to longitudinal accuracy, while the best theoretical accuracy is achieved when teleporting close to the maximal range of the given velocity. Especially for larger velocities, however, teleporting close to the maximal range becomes challenging as the target location is far away, hard to detect, and lateral hand-jitter increases. The limited resolution of even modern head-mounted displays is likely to negatively affect this even further. We can also see that the straight ray always has worse accuracy than the arc with the steepness approaching infinity towards 0° . So, while it is technically more accurate in the longitudinal axis to teleport as far as possible, it is also quite difficult to do so in practice since lateral accuracy decreases with distance. In our user study described in Section 4, we will therefore analyze the target selection behavior of users and discuss the results regarding these theoretical implications. To formalize our analysis, the following section outlines some fundamentals regarding Fitts' Law and its application to teleportation, which we used in a variation as an additional evaluation instrument.

3.2 Fitts' Law

Fitts' Law is a common model used in human-computer interaction to analyze the interplay of selection distance, movement time, and accuracy [21], [22], [51]. The core concept of Fitts' Law is that *movement time* (*MT*) can be modeled as a function of the distance to a target (referred to as *amplitude* (*A*) or *distance* (*D*)) and the size of the target (referred to as *target width* (*W*)). Each selection task is associated with

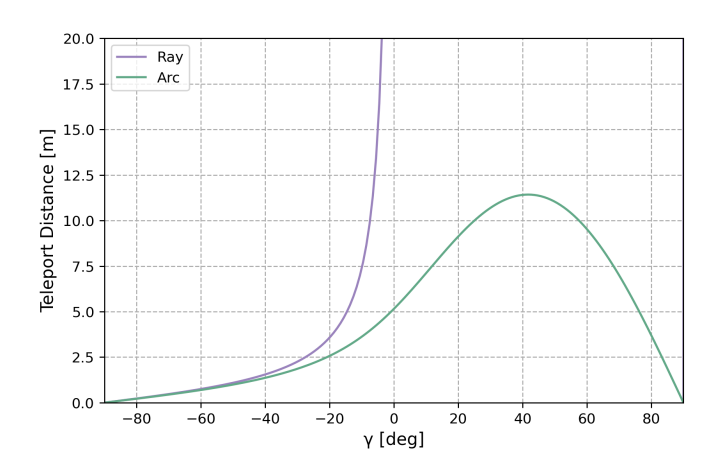


Fig. 3. Relationship between controller angle and teleportation distance for a parabolic arc (green) and a straight ray (purple). For the arc, an initial velocity of $10\frac{m}{2}$ and a controller height of 1.3~m was used. A controller angle of -90° corresponds to the controller pointing straight down, while an angle of 0° corresponds to the controller being aligned horizontally.

an *index of difficulty (ID)* calculated from D and W. A higher ID is associated with a more difficult selection, potentially increasing MT. The ID value can, therefore, be helpful as it encapsulates the selection difficulty that emerges from the angle–distance relationship discovered in the previous section into a single parameter.

While the original Fitts' Law model was developed for 1D reciprocal tapping and 2D pointing tasks, Kopper et al. adapted Fitts' Law for distal pointing tasks [32]. Cha and Myung showed that it can also be adapted to 3D pointing tasks [10]. Instead of using Euclidean coordinates to calculate D and W, both Kopper et al., and Cha and Myung used spherical coordinates. Therefore, D and W become angular values. Clark et al. further demonstrated that Fitts' Law can also be applied to selection tasks in VR [13]. For a more systematic overview of the use of Fitts' Law in XR, refer to Amini et al. [1].

We use the Shannon formula to calculate ID based on the paper about best practices for Fitts' Law from Soukoreff et al. [51] in bits:

 $ID = log_2\left(\frac{D}{W} + 1\right) \tag{9}$

In our case, D and W are angular values, where D corresponds to the distance the controller rotates from a defined starting point to the final position to teleport onto a platform. W corresponds to the angular width of the selected platform (see Figure 4) and encapsulates the longitudinal accuracy discussed in the previous section.

According to Soukoreff et al. [51], the ID should be adjusted for accuracy, which essentially reduces the target width. The adjustment for accuracy can be made with the error rate, and the *adjusted target width* (*We*) can be calculated with the following formula, as suggested by Soukoreff et al. [51]:

$$We = \begin{cases} W \times \frac{2.066}{z(1 - \text{Err}/2)}, & \text{if Err} > 0.0049\%, \\ W \times 0.5089, & \text{otherwise.} \end{cases}$$
(10)

where z(x) represents the inverse of the standard normal cumulative distribution or z-score, and Err the error rate

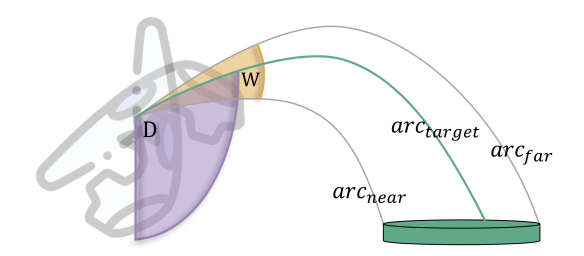


Fig. 4. Width and distance parameters to calculate the index of difficulty. For the selection process during teleportation, target distance D and target width W are angular values. D is the angular rotation of the controller from a defined starting position to the final position when the user executes the teleport (arc_{target}) . W is the difference between the controller angle required to get arc_{far} and arc_{near} and denotes the width of the target platform.

of the selection task. The *adjusted index of difficulty (IDe)* is then calculated using the Shannon formula and the adjusted target width.

$$IDe = log_2 \left(\frac{D}{We} + 1 \right) \tag{11}$$

To compare different selection devices, the IDe can be divided by the time required to execute the selection (*movement time* (*MT*)) to calculate a *throughput* (*TP*) value [22], [51]:

$$TP = \frac{IDe}{MT} \tag{12}$$

given in $\frac{bits}{s}$.

In Fitts' Law studies, the throughput value measures selection efficiency and can be used to compare different selection devices. In the context of teleportation, we understand efficiency as the ability to quickly reach a target location. This can be achieved by either making multiple short teleportations or by doing fewer longer ones. Similar to repeated selection tasks, there is always an initial delay before the next selection process begins. For teleportation, this delay can be expected to be longer than for repeated selection tasks because users need to reorient themselves after each teleportation. Additionally, if the transition is not instantaneous, this delay increases even further. The delay affects the overall movement time towards a goal destination, but is not modeled in the calculation of the throughput value of a single teleport. Because this delay is affected by multiple factors, it seems promising to maximize the selection distance of individual teleports. In practice, this means that, if it takes a user two seconds to select a target five meters away and one second of reorientation after each teleport, but only three seconds to select the final target 15 meters away, it is more efficient to spend the extra time during selection. In order to model this as an alternative to the classic throughput value of Fitts' Law, we suggest replacing movement time with teleportation distance in Equation 12. Additionally, the fraction has to be flipped so that higher values reflect that a teleport technique can be used to teleport farther without sacrificing accuracy. This results in the following formula to calculate our suggested teleport performance metric (TPM) given in [m/bits]:

$$TPM = \frac{TD}{IDe} \tag{13}$$

The TPM value thereby increases if either the teleportation distance increases or if the selection difficulty given by the IDe value decreases. In other words, the teleport parametrization with the best teleport performance offers the best trade-off between maximizing teleportation distance and minimizing the corresponding increase in index of difficulty. We will use this value later to analyze the different conditions in our user study.

3.3 Summary

In this section, we took a closer look at the mathematical background of the target selection process. The most important aspect of the target specification process is moving and rotating the controller until the arc intersects with the desired target location. Since the angle-distance relationship is not linear, the theoretical best longitudinal accuracy is achieved when teleporting close to the maximal range. In VR, however, it might be challenging to teleport to targets at greater distances as targets become harder to see and lateral hand jitter increases. It is, therefore, not clear how these theoretical implications hold in a practical VR use case. Consequently, we conducted a user study to understand the influence of different velocities, which directly influence the maximal teleportation distance, on accuracy and selected teleportation distance. In our analysis, we will use our novel teleport performance metric derived from Fitts' Law's throughput value to compare the different conditions in our user study.

4 USER STUDY

We believe that the way users teleport heavily depends on the environment at hand. For example, it is very likely that in a small indoor environment, a lower maximal reach would be better as it is not necessary to teleport large distances, while in large open scenarios with only a small number of obstacles, larger values would be preferable to reach a target destination faster. However, longer distances are likely to also come with lower selection accuracy, and it is unclear at which point the entire selection process becomes infeasible.

Therefore, we conducted a within-subjects user study that tested the selection of teleportation targets with different projectile emission velocities in a worst-case scenario, which assumes that users want to teleport efficiently and therefore want to maximize the teleportation distance. Even if not all users do so in practice, this controlled scenario allowed us to determine upper distance bounds at which targets can still be selected accurately with different velocities. These thresholds can then be used to support system developers in choosing appropriate parameters for a particular use case. The independent variables of this study were the emission velocity $v_0 = \{6, 8, 10, 12, 14, 16, 18, 20, 22, \text{Infinity}\}$ and the size of the target platform (small, medium, large).

4.1 Task Design

Users were placed on a river with a sequence of platforms in the form of water lilies in front of them (see Figure 1 (d)). They were tasked to perform a teleport to the farthest

possible platform that they still felt comfortable selecting accurately. We spawned a total of 150 platforms for each teleportation, which makes the platforms visually appear to extend indefinitely along the river. To better see the platforms and to provide some variation, we introduced a small random jitter of at most one meter in the lateral direction of the river. Independent of the size of the platform, there was always a gap of $0.5\ m$ between each platform in the longitudinal direction of the river, requiring accuracy in this direction as well.

Before being able to select a target location, participants were prompted to point the controller to the ground, which can be seen in Figure 1 (b). The system checked if the angle of the controller was at $-90^{\circ} \pm 10^{\circ}$ for one second. This ensured that we always had a fixed starting point for the selection. The teleportation was done in two steps. While the trigger button was held, the arc was visualized, and users were able to aim at a platform. To be in line with our goal of creating a worst-case scenario, the color of the arc was chosen to be similar to the platforms, as this might also be the case in more realistic scenarios since the color of the arc is usually constant (e.g. [24], [39], [40], [52]). When the trigger button was released, the target location was confirmed. With the grab button on the side of the controller, the teleport could be aborted, so letting go of the trigger button would not result in a selection. If the selected target location was on a platform, users were teleported to that location, and a short sound was played to confirm the successful selection. If the target location was not on a platform, the teleportation would be considered as failed, and users would not be teleported. To encourage users to avoid a failed selection, a loud, unpleasant by design, error, and splash sound was played. Additionally, to encourage participants to select larger distances, we awarded a score based on the selected distance in meters. A failed teleportation would result in a point reduction of 15 m. Users could see the score they got for the last teleport at a display attached to the controller, which can be seen in Figure 1 (c). An overview of the whole environment can be seen in Figure 1 (a).

4.2 Independent Variables

In our user study, we tested ten different velocity values v_0 from 6 $\frac{m}{s}$ to 22 $\frac{m}{s}$ in increments of two resulting in a maximal reach of 5.07 m to 50.91 m and an "infinite" velocity condition to simulate straight-ray selection as a baseline. These values cover the teleportation distances reported in most papers we presented in Section 2. Smaller velocities were deemed uninteresting as the maximal teleport distance became trivially small. We also included larger velocities to find an upper limit for the accurate selection capability with parabolic arcs. The mathematical maximal range and the optimal angle to reach it for each velocity are given in Table 1, which was calculated using Equation 7 and Equation 8 using the logged average values for the controller's position $d_{max}(v_0, 0.27, 1.30)$.

Across the different velocity conditions, platforms appeared in three different sizes ($d_{small}=0.4\ m,\ d_{medium}=0.8\ m,\ d_{large}=1.2\ m$) to vary the selection difficulty of the task. The smallest size represented an average user's

minimum space required to be able to stand, based on the average shoulder width of humans⁵. The larger platforms were scaled to twice and thrice the size of the smaller platform to linearly increase the required accuracy and selection difficulty. While we acknowledge that human scale perception might increase exponentially, we disregarded even larger platforms based on initial pilot tests that demonstrated that sizes beyond the largest platform resulted in highly trivial selection tasks.

4.3 Dependent Variables

For each teleport, we logged the following parameters: 1) The controller angle before the start of the selection to calculate the distance value for the index of difficulty calculation; 2) the teleport distance, given as the difference from the selected target location to the initial position of the user; 3) if the teleport was successful. A teleportation was classified as successful if the target location lay on a platform. The platform is then referred to as the selected platform; 4) the position and size of the selected platform to be able to calculate the target width for the index of difficulty value; and 5) the position and rotation of the controller at the time the teleport was executed.

4.4 Hypotheses

Based on the logged data and research question, we formulated the following hypotheses before the user study:

- H₁: There is a projectile velocity threshold beyond which the selected distances will not get larger.
- H₂: Selected distances will be higher when larger platforms are offered.
- H_3 : Smaller velocities will be associated with higher controller heights.
- H_4 : The number of failed teleports will increase with larger velocities.
- H_5 : The number of failed teleports will increase when smaller platforms are offered.
- H_6 : The selection performance of the straight ray will be different from the parabolic arc.

We hypothesized that there is a visual bottleneck for larger distances, only possible with higher velocities, where participants cannot clearly see the arc's end anymore and whether it is on a platform (H_1) . This effect is more prominent when teleporting onto smaller platforms, increasing the failure rate (H_2, H_4, H_5) . For smaller velocities, the possible teleportation distance is very small, so we hypothesized that participants would compensate for this by holding the controller higher to potentially reach the next available platform (H_3) . The straight ray is very prone to jitter, as discussed in Section 3.1.1 (see Figure 3), and as the ray intersects with the platforms at a flatter angle, the intersection point becomes less visible. We, therefore, hypothesized that the selection performance, in general, will be different from the parabolic ray (H_6) .

5. Data taken from https://iba.online/knowledge/en/raeume-planen/office-planning/body-dimensions/ based on DIN 33402-2

4.5 Apparatus

The application was developed using the Unity game engine (Version 2022.3.29). For data logging during the user study, the *Unity Experiment Framework* was used [8]. The application was packaged as an .apk file and was installed on a Meta Quest 3 headset running in standalone mode with the included controllers. An aftermarket head strap was added to allow users to adjust the headset better. The physical space was approximately $3\ m\times 3\ m$. However, participants were instructed to remain stationary in this space. The application ran at the standard resolution of the headset $(2,064\times 2,208\ \text{pixels}\ \text{per}\ \text{eye})$ at a fixed refresh rate of 72 frames per second. To improve the reproducibility, we made the .apk file of our application publicly available [46].

4.6 Participants

For the user study, we recruited 60 participants (30 male, 30 female), who were mainly computer science students between 19 and 53 years old ($M=26.63, \sigma=6.23$) from two different universities. 49 participants had prior VR experience, out of which 32 do not use VR regularly. Out of the remaining 17 participants who use VR regularly, five did so for less than one year, four for one to two years, three for two to four years, and five for more than four years. We also asked the 49 participants who had already used VR before to rate their skill level with using VR technology (Beginner: 26, Advanced: 8, Competent: 6, Proficient: 6, Expert: 3) and what interface they have used before (Teleportation: 35, Steering: 26, Object-selection via straight ray: 28, it was possible to select multiple options).

4.7 Procedure

The user study was conducted at two different universities following the same procedure to recruit a larger and more diverse participant pool. Upon arriving at the laboratory, participants read the task description, drew a random number to which the logged data was linked, and were introduced to the controls. In addition to a written description, participants also got a verbal introduction about the task and the goal. Participants were told that they should teleport as far as possible to get a large score but should avoid failing to accurately hit a platform as that would result in a large point penalty. They were also told that time was not important. Afterward, they put on the headset, entered their unique number, and started with a practice task where they had to perform 10 successful teleportations. The velocity during the practice task was the same as in the first condition to mitigate learning effects. Afterward, 10 conditions followed, each with a different velocity. To complete a condition, every participant had to perform 18 successful teleports. The order of the conditions was randomized between participants. The size of the platforms changed after each teleport in a counterbalanced random order to ensure that six successful teleports were performed for each velocity-platform combination. After each condition, participants were offered a short optional break. After completing all ten conditions, participants filled out a demographics questionnaire on a tablet. In total, the user study took 30 to 60 minutes to complete, and participants were

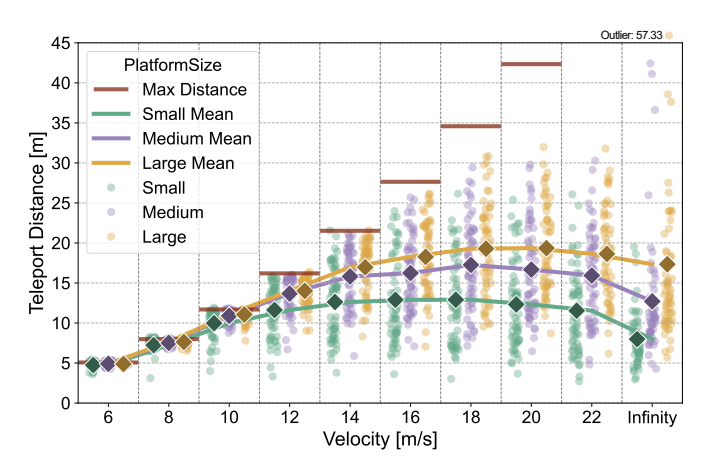


Fig. 5. Plot of the teleport distance in meters over all velocities. The dots indicate the average value per user and are color-coded for each platform size. Lines and diamonds represent the average teleport distance over all users for each velocity and platform size. Note that the diamonds and dots are jittered along the x-axis for better visibility, while the lines are rendered in the center of each velocity column. The red lines mark the maximal teleport distance for each velocity calculated with Equation 8 $(d_{max}(v_0,0.27,1.30)).$

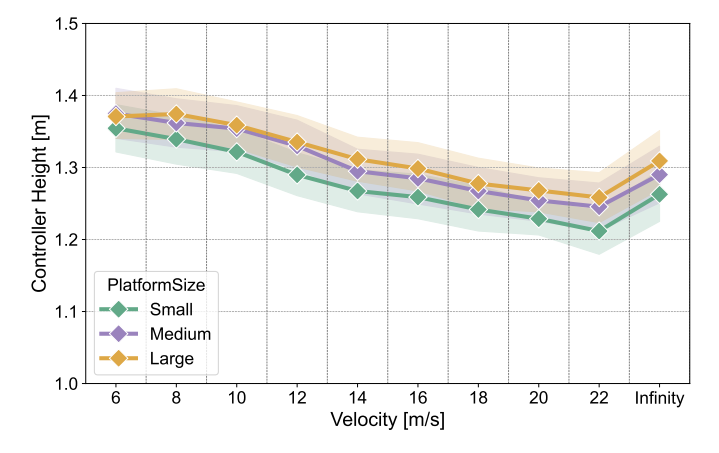


Fig. 6. Plot of the controller height in meters over all velocities. Diamonds indicate the average value over all users for each velocity color-coded for each platform size. The area around the lines indicates the 95% confidence interval.

rewarded 10 Euros as compensation. The study procedure, including data acquisition and handling, was approved by the ethics board of Trier University (no. 10/2023).

4.8 Results

For a general overview of our results, we calculated the mean and standard deviations of the dependent variables, which can be seen in Table 1. To visualize our results, we created plots using Python and Matplotlib [28]. We used the statistics tool Jamovi [29] for further statistical analysis of our dependent parameters with a significance level of 5%. We assumed a normal sampling distribution of our data based on our sample size of N=60 in the context of the central limit theorem [20, pp. 170–172]. Our data files are provided as supplemental material for additional clarity [47].

Teleport Distance: For the teleport distance measure, we created a plot split by the platform size (Figure 5).

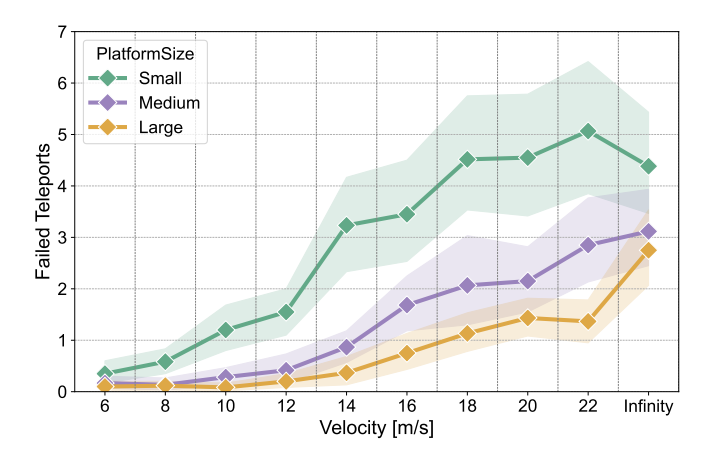
We also conducted a repeated measures ANOVA with the factor velocity and platform size for the teleport distance, showing a significant main effect of platform size: $F(2,118)=108.38,\ p<0.001,\ \eta_p^2=0.648$ (large effect), velocity: $F(9,531)=116.78,\ p<0.001,\ \eta_p^2=0.664$ (large effect) and the interaction effect platform size \times velocity: $F(18,1062)=6.63,\ p<0.001,\ \eta_p^2=0.101$ (medium effect). Since we did not formulate hypotheses about individual velocities and because of the large number of conditions, we omitted further pairwise post-hoc tests.

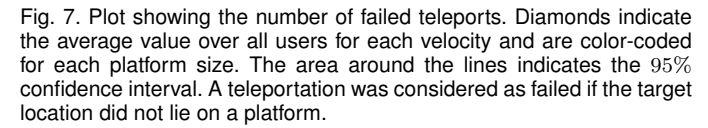
To further describe the relationship between different velocity settings, we calculated the effect size of adjacent velocities (Table 2). We labeled effect sizes that are $d \leq 0.1$ to indicate that there is not even a small effect. A small effect is indicated by values above d=0.2, so we considered values half of that to be a valid indication that the differences are merely marginal. To get an idea about the general influence of the platform size on teleportation distance over all velocities, we calculated mean, standard deviation, and 95% confidence intervals for the three platform sizes over all velocities (small: N=600, M=10.4, SD=4.78, CI[10.0; 10.8], medium: <math>N=600, M=13.2, SD=5.88, CI[12.7; 13.6], large: <math>N=600, M=14.7, SD=7.82, CI[14.1; 15.4]). The fact that the confidence intervals do not overlap indicates substantial differences in teleport distance between platform sizes.

Controller Height: For the controller height, we created a plot (Figure 6) and performed a linear regression analysis with the controller height over all platform sizes as the dependent variable and velocity—excluding infinity (N=540)—as a covariate. A significant regression was found (F(1,538)=68.7,p<.001). The R^2 was 0.11, indicating that the velocity explained approximately 11% of the variance of the controller height.

Failed Teleports: The number of failed teleports for each velocity and platform was plotted with 95% confidence intervals (Figure 7). In addition, we performed a linear regression analysis with the number of failed teleports over all platform sizes as the dependent variable and velocity excluding infinity (N = 540)—as a covariate. A significant regression was found (F(1, 538) = 184, p < .001). The R^2 was 0.26, indicating that the velocity explained approximately 26% of the variance of the number of failed teleports. To get an idea about the general influence of the platform size on the number of failed teleports over all velocities, we calculated mean, standard deviation, and 95% confidence intervals for the three platform sizes over all velocities (small: N = 600, M = 2.89, SD = 3.81, CI[2.58; 3.19],medium: N = 600, M = 1.37, SD = 2.39, CI[1.18; 1.56],large: N = 600, M = 0.83, SD = 1.64, CI[0.70; 0.96]). The fact that the confidence intervals do not overlap indicates substantial differences in the number of failed teleports between platform sizes.

Index of Difficulty: A plot was created for the adjusted index of difficulty, which was calculated based on Equation 11 (Figure 8). The plot is not separated into platform size as the index of difficulty value already incorporates the platform size. To show that the index of difficulty increases with increasing velocity, we performed a linear regression analysis with the adjusted index of difficulty as the dependent variable and velocity—excluding infinity





(N=540)—as a covariate. A significant regression was found (F(1,538)=736,p<.001). The R^2 was 0.58, indicating that the velocity explained approximately 58% of the variance of the adjusted index of difficulty.

Teleport Performance: As discussed before in Section 3.2, our results showed that movement time did not drastically change between different velocities, and therefore Fitts' Law's throughput value does not provide enough insight to compare the different conditions (we reported mean and standard deviations for both values in Table 1). The smallest movement time was $M=3.39,\ \sigma=1.31$ at $6\frac{m}{s}$) and the largest $M=4.37,\ \sigma=2.00$ at $16\frac{m}{s}$). Therefore, to analyze the teleport performance, we used our teleport performance metric derived in Section 3.2 and created a plot for each velocity (Figure 9). As the teleport performance metric is calculated based on the adjusted index of difficulty, it is also not split into platform sizes. Similar to the teleport distance, we wanted to formalize what can be seen visually in the plot and, therefore, also calculated effect sizes of adjacent velocities (Table 2). Similar to teleport distance, we also labeled effect sizes that are $d \leq 0.1$ to indicate that differences are marginal.

5 DISCUSSION

In this section, we will discuss the results from the user study regarding the hypotheses and findings from the mathematical background discussed in Section 3. We will first exclude the straight ray or infinite velocity condition from our analysis and revisit it in a separate paragraph where we discuss the general differences between the parabolic arc and the straight ray (H_6) .

5.1 Hypotheses

Selection Distance (H_1 and H_2): From the teleport distance plot in Figure 5, we can see that for all platform sizes, there is an increasing phase at lower velocities and a maximal point after which the teleportation distance decreases again. This is underlined by the effect sizes of adjacent velocities seen in Table 2. The table shows that while effect sizes are large

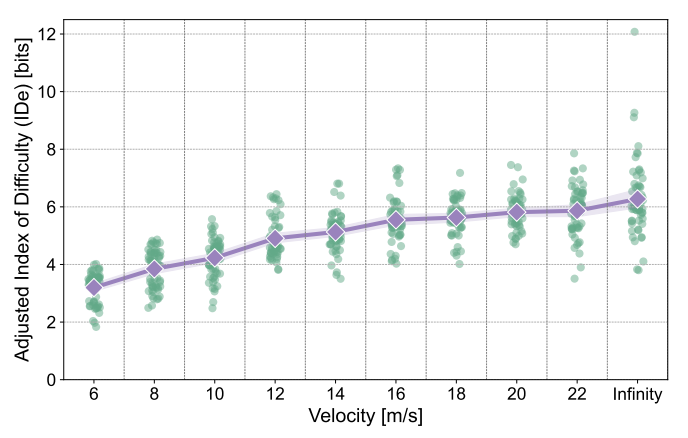


Fig. 8. Plot of the adjusted index of difficulty value over all velocities calculated using Equation 11. Dots indicate the individual results of each user. Diamonds indicate the average value over all users for each velocity. The area around the lines indicates the 95% confidence interval.

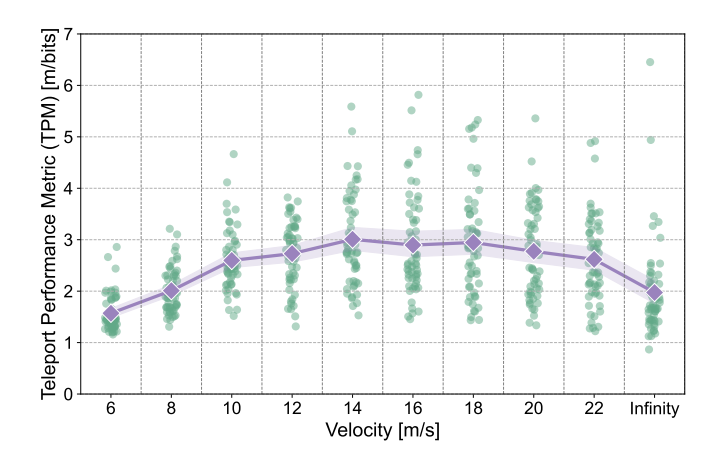


Fig. 9. Plot of our novel teleport performance metric over all velocities calculated using Equation 13. Dots indicate the individual results of each user. Diamonds indicate the average value over all users for each velocity. The area around the lines indicates the 95% confidence interval.

for small velocities, the differences become very small (less than half of a small effect size) starting at $14~\frac{m}{s}$ for small and medium platforms and at $18~\frac{m}{s}$ for larger platforms. The sign of the effect size also changes, indicating that the selection distance first rises to a maximum before values get smaller again. The results from the repeated measures ANOVA further indicate that velocity, platform size, and the interaction effect of both have a significant influence on the teleportation distance. We can, therefore, confirm H_1 , stating that there is a projectile velocity threshold beyond which the selected distances will not get larger.

Additionally, we calculated the confidence intervals over all velocities for the teleportation distance for small, medium, and large platforms. The fact that confidence intervals do not overlap shows that the platform size has a substantial influence on the teleport distance, with the highest selection distance achieved when larger platforms are offered. We can, therefore, confirm H_2 , stating that selected distances will be higher when larger platforms are offered.

The results show that there is a velocity threshold be-

TABLE 1

Mean and standard deviations for dependent parameters. *: N=6 teleports per platform size \cdot 60 users = 360, †:

N=18 teleports $\cdot 60$ users $=1080, \ddagger: N=60$ users. **Optimal angle** γ_{opt} to reach the **maximal distance** d_{max} for each velocity calculated using Equation 7 and Equation 8 with the average values of the controllers' position logged during our study $(x_0=0.27,y_0=1.30)$. The angle is thereby in reference to the horizontal plane, so an angle of 0° corresponds to the controller's forward vector being parallel to the horizontal plane. **Teleport distance** is the distance from the user's position to the selected target location in meters. **Failed teleports** refers to the number of failed teleports. A teleport is considered failed if the selected target location is not on a platform. **ID** is the index of difficulty value calculated using Equation 9 in bits. **IDe** is the adjusted index of difficulty value calculated using Equation 11 in bits. Only one IDe value is calculated per user per velocity since the calculation relies on the failure rate. **MT** is the average movement time in seconds for every user. **TP** is the throughput value calculated using Equation 12. **TPM** is a novel teleport performance metric that is calculated by dividing the teleportation distance by the adjusted index of difficulty given in meters per bits. Note that for the Fitts' Law parameters, the results are not grouped by platform size as this is encapsulated in the index of difficulty parameter.

v ₀ [m/s]	6		8		10 12		2 14		16		18		20		22		Infinity			
γ_{opt} [deg]	37.42		40.22		41.75		42.67		43.25		43.64		43.92		44.12		44.26		0	
d_{max} [m]	5.07		7.99		11.69		16.20		21.52		27.64		34.58		42.34		50.91		∞	
	Mean	SD	Mean	SD	Mean	SD	Mean	SD	Mean	SD	Mean	SD	Mean	SD	Mean	SD	Mean	SD	Mean	SD
Platform Size	Teleport Distance* [m]																			
Small	4.74	0.38	7.23	0.75	9.98	1.71	11.63	3.07	12.62	4.40	12.90	5.24	12.91	5.46	12.32	5.43	11.54	5.34	7.98	3.40
Medium	4.91	0.29	7.52	0.34	10.90	0.73	13.67	2.16	15.81	3.51	16.24	4.57	17.26	5.55	16.67	5.76	15.93	5.75	12.71	7.34
Large	4.88	0.17	7.63	0.42	11.06	0.79	14.02	1.69	16.96	3.23	18.27	4.58	19.29	5.80	19.36	5.50	18.63	5.71	17.34	15.54
Platform Size	Failed Teleports*																			
Small	0.35	0.90	0.58	0.94	1.20	1.79	1.55	1.75	3.23	3.61	3.45	3.92	4.52	4.32	4.55	4.49	5.07	5.05	4.38	4.14
Medium	0.17	0.49	0.13	0.47	0.28	0.64	0.42	1.11	0.87	1.24	1.68	2.11	2.07	3.46	2.15	2.63	2.85	3.16	3.12	2.99
Large	0.10	0.35	0.12	0.32	0.08	0.28	0.20	0.58	0.37	1.07	0.75	1.39	1.13	1.51	1.43	1.49	1.37	1.69	2.75	3.07
Platform Size									Cor	troller	Height*	[m]								
Small	1.35	0.13	1.34	0.13	1.32	0.12	1.29	0.12	1.27	0.12	1.26	0.12	1.24	0.13	1.23	0.10	1.21	0.12	1.26	0.14
Medium	1.37	0.14	1.36	0.14	1.35	0.13	1.33	0.14	1.29	0.12	1.28	0.13	1.27	0.13	1.25	0.12	1.25	0.13	1.29	0.15
Large	1.37	0.13	1.37	0.13	1.36	0.13	1.34	0.14	1.31	0.12	1.30	0.14	1.28	0.14	1.27	0.12	1.26	0.14	1.31	0.16
									Fitts'	Law										
ID† [bits]	2.68	0.18	3.45	0.26	4.02	0.41	4.97	0.32	5.60	0.35	6.13	0.26	6.44	0.36	6.67	0.40	6.73	0.61	7.29	1.39
IDe [‡] [bits]	3.20	0.54	3.84	0.67	4.23	0.67	4.91	0.68	5.13	0.66	5.55	0.75	5.63	0.60	5.82	0.58	5.86	0.83	6.27	1.31
MT [‡] [s]	3.39	1.31	3.88	1.62	3.94	1.48	4.16	1.55	4.24	1.37	4.37	2.00	4.23	1.65	4.20	1.89	4.05	1.70	4.09	1.72
TP ‡ [bits/s]	1.07	0.42	1.13	0.41	1.22	0.47	1.36	0.57	1.33	0.43	1.47	0.57	1.49	0.48	1.59	0.54	1.62	0.52	1.71	0.53
TPM [‡] [m/bits]	1.57	0.35	2.01	0.43	2.60	0.58	2.73	0.62	3.01	0.87	2.90	0.97	2.95	1.00	2.77	0.88	2.62	0.85	1.97	0.89

TABLE 2 Effect sizes between adjacent velocity conditions. Green cells indicate marginal differences $(d \leq 0.1)$. * indicate that pairwise t-tests showed significant differences (p < 5%).

v ₀ [m/s]	6/8	8/10	10/12	12/14	14/16	16/18	18/20	20/22	22/Inf				
Platform Size	Effect Size Teleport Distance												
Small	-2.92*	-1.36*	-0.46*	-0.20	-0.04	< 0.01	0.08	0.11	0.57*				
Medium	-6.26*	-3.91*	-1.20*	-0.51*	-0.07	-0.15	0.07	0.10	0.33*				
Large	-5.99*	-3.53*	-1.60*	-0.90*	-0.22	-0.13	-0.01	0.10	0.07				
•	Effect Size Teleport Performance Metric												
	-0.846*	-0.839*	-0.154	-0.277	0.094	-0.040	0.136	0.133	0.531*				

yond which the selection distance decreases again. This can also be explained by the angle-distance relationship introduced in Section 3.1.1, which showed that the accuracy is higher when users teleport closer to the maximal range. In the user study, for higher velocities, users selected platforms that were far away from the maximal distance. To select these closer locations, the controller's rotation angle was smaller than γ_{ont} , therefore moving more to the steeper side of the angle-distance curve in Figure 3, which reduces the longitudinal accuracy and made selection harder, which likely also resulted in users selecting closer platforms. The reduced accuracy and, therefore, more difficult selection can also be seen in the resulting plot of the adjusted index of difficulty in Figure 8, where the linear regression showed a significant increase in selection difficulty towards higher velocities.

Controller Height (*H*₃): From the controller height plot in Figure 6, we can see that the controller height decreases over the parabolic arc conditions independent of the platform size. The linear regression over all platform sizes

further showed a significant effect. We, therefore, confirm H_3 , stating that *smaller velocities will be associated with higher controller heights*. The results can potentially be explained by the projectile motion equation where the initial controller height y_0 positively contributes to the maximal teleportation range (see Equation 8). Therefore, users potentially compensated for the small teleport distance at lower velocities by raising the controller to be able to reach the next platform. However, the linear regression showed that the influence of the velocity only accounted for 11% of the variance of the controller height, so there must be other factors as well.

Number of Failed Teleports (H_4 and H_5): From Figure 7, we can see that the number of failed teleports generally increases with the velocity. The linear regression over all platform sizes further showed a significant effect. Additionally, we calculated confidence intervals over all velocities for the number of failed teleports, showing a strong influence of the platform size since the confidence intervals do not overlap between different platform sizes. Small platforms consistently resulted in more failed teleports than medium and large platforms, respectively, for each velocity. We can, therefore, confirm H_4 and H_5 , stating that the number of failed teleports will increase with larger velocities and increase when smaller platforms are offered. Overall, the increase in failed teleports can also be explained by the distance-accuracy relationship as the controller's rotation is further away from γ_{opt} , and therefore, on the steeper section of the distance– accuracy curve (see Figure 3), which reduces the accuracy, results in a higher index of difficulty value and therefore an increase in failure rate.

Parabolic Arc vs. Straight Ray (H_6): So far, we have

excluded the straight ray or infinite velocity condition from our discussion. Combining the results of several dependent variables allows for a more detailed comparison of the straight ray compared to its parabolic counterparts. In the teleport distance plot in Figure 5, the distance further decreases from $22 \frac{m}{s}$ to infinity, which is consistent with our representation of the straight ray as a projectile with infinite emission velocity. In the failed teleports plot in Figure 7, we can see a similar trend. Although the bump from $22 \frac{m}{2}$ to infinity is most drastic for large platforms, it also holds for medium-sized platforms. Interestingly, the error rate decreases from the $22 \frac{m}{s}$ condition to the straight ray condition when small platforms are offered. A potential explanation for this effect can be found by looking at the index of difficulty plot. The straight ray has the highest selection difficulty, and smaller platforms result in an even higher index of difficulty value. To compensate for this, users selected closer platforms, which can be seen in the teleport distance plot where users only selected targets at an average distance of 7.98 m, when small platforms were offered, which drastically differs from the $22 \frac{m}{s}$ condition where users still teleported an average of 11.54 m) for small platforms. Because these smaller, closer platforms are easier to select, the failure rate decreases. The selected distance for the straight ray for small platforms is similar to that of the $8 \frac{m}{s}$ velocity condition, although the failure rate differs drastically (0.58 for $v_0 = 8 \frac{m}{s}$ vs. 4.38 for $v_0 = \infty \frac{m}{s}$ failed teleports for infinity), which further shows that the straight ray has a high selection difficulty.

A similar explanation can potentially be given for the increase in controller height from $22 \, \frac{m}{s}$. For the straight ray, the intersection angle between the ray and the platform is very flat for larger selection distances, which increases the index of difficulty. To counteract this, participants selected closer platforms and held the controller higher to increase the intersection angle. Both adjustments decrease the index of difficulty value, making the selection easier.

All of this leads us to the conclusion that the straight ray extends the trends shown for increasing velocities. We would, therefore, reject H_6 , stating that the selection performance of the straight ray will be different from the parabolic ray.

Optimal Velocity: The fact that the teleport distance plot in Figure 5 shows that there is a plateau after which selection distance decreases again indicates that there must be an optimal velocity beyond which selection performance gets worse. To find this optimal velocity, we plotted our novel teleport performance metric (Figure 9). From the change in effect sizes seen in Table 2 and the plot, we can see that there is a plateau between $14 \frac{m}{s}$ and $18 \frac{m}{s}$ where the highest teleport performance is achieved. With these velocities, the maximal teleportation distance ranges between $d_{max}(14, 0.27, 1.30) = 21.52 \text{ m} \text{ and } d_{max}(18, 0.27, 1.30) =$ 34.58 m, which is higher than nine of the twelve papers we covered in Section 2.2.1. Based on the angle-distance relationship, showing that accuracy is highest when teleporting close to the maximal reach and the fact that we tested for the maximal feasible teleportation distance, we suggest using the smallest value, as we would expect users to teleport to closer distances in a realistic scenario. Therefore, we conclude that a velocity of $14 \frac{m}{s}$ has the best trade-off between selection distance and accuracy with a teleport

performance of $TPM=3.01\frac{m}{bits}$. This means that for every increase in the index of difficulty of 1 a user is willing to accept during selection, they will gain an average of 3.01~m in teleportation distance.

5.2 Take-Home Message

If accuracy is of importance during teleportation, our results suggest that values beyond a velocity of $18~\frac{m}{s}$ ($d_{max}(18,0.27,1.30)=34.58~m$) result in a reduced teleport performance. Furthermore, if teleportation behavior cannot be predicted due to changing environments, we suggest using $14~\frac{m}{s}$ ($d_{max}(14,0.27,1.30)=21.52~m$) as parametrization for the initial velocity of the teleport parabola, as this value yielded the best tradeoff between maximizing selected teleportation distance and accuracy. We cannot recommend using a straight ray as a target selection mechanism during teleportation as its poor accuracy limits performance.

5.3 Limitations

We acknowledge that the study was conducted under controlled conditions, which may limit ecological validity. However, this level of control was necessary to isolate the influence of the initial projectile velocity on the selection distance and accuracy and establish a clear causal relationship. Establishing such effects under controlled conditions is an essential first step before moving toward more complex, ecologically valid settings in future research. For example, our virtual environment did not include any elevation changes, rotation, or scale specification; it only required people to teleport forward and used a stylized rendering. In addition, our user study scenario can be seen as a "worstcase scenario", as we assumed that participants want to teleport accurately and far at the same time. It is unclear how the results change in applications where all teleports have to be performed in a similar distance range. In other words, if application designers can predict how far users will teleport beforehand, e.g., based on the size of the environment, they should pick a velocity that has a maximal teleport distance around the expected value based on the angle-distance relationship (see Figure 3) to maximize accuracy. Designers can refer to Table 1 to pick an appropriate velocity based on the expected teleport distance. Especially for very small environments, lower velocity values than our suggested optimal value of $14 \frac{m}{s}$ might work better. In our user study, we assumed that users wanted to remain accurate during the target selection, which might not always be the case. If accuracy is not of importance, higher velocity values can be chosen as well, which would increase efficiency as larger distances can be traversed quicker.

Finally, we considered teleportation distance to be a larger factor for teleport performance than specification time, since the specification time was fairly constant throughout the different conditions. In general, our proposed teleport performance metric is just a first step in modelling efficient target selection, and there might be alternative ways to calculate it. It serves as an addition to Fitts' Laws throughput value, and designers should evaluate which metric better suits their purpose.

6 CONCLUSION AND FUTURE WORK

Our research question asked about the influence of the maximal reach of the teleport parabola on selection distance and accuracy. Our theoretical results showed that longitudinal selection accuracy is maximized when teleporting close to the mathematical maximal range as given by the angledistance relationship. Our user study, however, showed that although higher velocities would allow for farther teleportations, there is a projectile velocity threshold beyond which the selected distances will not get larger anymore. Interestingly, the user-selected teleportation distance decreases for larger velocities and the straight ray, indicating that there is an optimal velocity beyond which selection becomes too difficult, resulting in participants selecting closer targets. To get further insights into this, we also calculated *index of difficulty* values for each teleport and compared the selected index of difficulties to the teleportation distance to get a performance measure for teleportation (similar to the throughput value in a traditional Fitts' Law analysis [51]), which can potentially be used to compare different teleportation techniques in the future. The results indicate that there is an optimal velocity threshold at $14 \frac{m}{s}$ beyond which teleportation performance

Similar to previous implementations, our selection arc follows physical laws. In VR, however, we do not need to conform to the laws of physics. Therefore, in the future, it might be interesting to explore alternative arcs. The user could also manually adjust the desired teleportation distance, and the system could then automatically alter the velocity or the gravity to an optimal value. In addition, since the angle-distance relationship is not linear as discussed in Section 3.1.1, in the future, it might be interesting to analyze different functions, for example, a linear function or even higher-order functions, to potentially increase accuracy during selection. To further improve the accuracy of the target selection process, enhancements could be provided in the form of, e.g., a preview of the target location, which would mitigate the visual bottleneck of the selection process. In addition, an input smoothing algorithm could be used to decrease hand jitter associated with long teleportations. Regarding our proposed teleport performance metric, we argued that movement time is less important than teleportation distance for the efficiency of individual teleports, because classic Fitts' Law does not model the delay between teleports. In the future, a more sophisticated metric could model these delays by considering a sequence of required teleports to reach a goal location, rather than focusing only on individual ones. Furthermore, it will be interesting to add rotation specifications and include teleportations to different elevation or scale levels to see how these aspects would affect our results.

Overall, more detailed research on the design of teleportation techniques will provide a solid basis for the informed selection of parameters and mechanisms in the future.

7 ACKNOWLEDGEMENTS

This work has received funding from the German Research Foundation (Deutsche Forschungsgemeinschaft, DFG) under grant 528403131 (Project "Put me There").

REFERENCES

- [1] M. Amini, W. Stuerzlinger, R. J. Teather, and A. U. Batmaz. A Systematic Review of Fitts' Law in 3D Extended Reality. In Conference on Human Factors in Computing Systems, CHI '25, 25 pages, Apr 2025. doi: 10.1145/3706598.3713623
- [2] N. H. Bakker, P. O. Passenier, and P. J. Werkhoven. Effects of Head-Slaved Navigation and the Use of Teleports on Spatial Orientation in Virtual Environments. *Human Factors: The Journal of the Human Factors and Ergonomics Society*, 45(1):160–169, Mar. 2003. doi: 10. 1518/hfes.45.1.160.27234
- [3] J. Bhandari, P. MacNeilage, and E. Folmer. Teleportation without Spatial Disorientation Using Optical Flow Cues. In *Proceedings of Graphics Interface 2018*, Gi 2018, 6 pages, pp. 162 – 167. Canadian Human-Computer Communications Society / Société canadienne du dialogue humain-machine, 2018. doi: 10.20380/gi2018.22
- [4] C. Boletsis and J. E. Cedergren. VR Locomotion in the New Era of Virtual Reality: An Empirical Comparison of Prevalent Techniques. Advances in Human-Computer Interaction, 2019(1):7420781, 2019. _eprint: https://onlinelibrary.wiley.com/doi/pdf/10.1155/2019/7420781. doi: 10.1155/2019/7420781
- [5] D. Bowman, D. Koller, and L. Hodges. Travel in Immersive Virtual Environments: An Evaluation of Viewpoint Motion Control Techniques. In *Proceedings of IEEE 1997 Annual International Symposium on Virtual Reality*, pp. 45–52, IEEE Comput. Soc. Press, Albuquerque, NM, USA, 1997. doi: 10.1109/vrais.1997.583043
- [6] E. Bozgeyikli, A. Raij, S. Katkoori, and R. Dubey. Point & Teleport Locomotion Technique for Virtual Reality. In *Proceedings of the 2016* Annual Symposium on Computer-Human Interaction in Play, Chi Play '16, 12 pages, p. 205–216. Association for Computing Machinery, New York, NY, USA, 2016. doi: 10.1145/2967934.2968105
- [7] E. Bozgeyikli, A. Raij, S. Katkoori, and R. Dubey. Locomotion in virtual reality for room scale tracked areas. *International Journal of Human-Computer Studies*, 122:38–49, 2019. doi: 10.1016/j.ijhcs.2018.08.002
- [8] J. Brookes, M. Warburton, M. Alghadier, M. Mon-Williams, and F. Mushtaq. Studying human behavior with virtual reality: The Unity Experiment Framework. *Behavior Research Methods*, 52(2):455–463, Apr. 2020. doi: 10.3758/s13428-019-01242-0
- [9] F. Buttussi and L. Chittaro. Locomotion in Place in Virtual Reality: A Comparative Evaluation of Joystick, Teleport, and Leaning. IEEE Transactions on Visualization and Computer Graphics, 27(1):125–136, 2021. doi: 10.1109/tvcg.2019.2928304
- [10] Y. Cha and R. Myung. Extended Fitts' law for 3D pointing tasks using 3D target arrangements. *International Journal of Industrial Ergonomics*, 43(4):350–355, July 2013. doi: 10.1016/j.ergon.2013.05. 005
- [11] L. A. Cherep, A. F. Lim, J. W. Kelly, D. Acharya, A. Velasco, E. Bustamante, A. G. Ostrander, and S. B. Gilbert. Spatial Cognitive Implications of Teleporting Through Virtual Environments. *Journal of Experimental Psychology: Applied*, 26(3):480–492, Sept. 2020. doi: 10.1037/xap0000263
- [12] C. G. Christou and P. Aristidou. Steering Versus Teleport Locomotion for Head Mounted Displays. In L. T. De Paolis, P. Bourdot, and A. Mongelli, eds., Augmented Reality, Virtual Reality, and Computer Graphics, pp. 431–446. Springer International Publishing, Cham, 2017. doi: 10.1007/978-3-319-60928-7_37
- [13] L. D. Clark, A. B. Bhagat, and S. L. Riggs. Extending Fitts' law in three-dimensional virtual environments with current low-cost virtual reality technology. *International Journal of Human-Computer Studies*, 139:102413, July 2020. doi: 10.1016/j.ijhcs.2020.102413
- [14] J. Clifton and S. Palmisano. Effects of steering locomotion and teleporting on cybersickness and presence in HMD-based virtual reality. *Virtual Reality*, 24(3):453–468, Sept. 2020. doi: 10.1007/ s10055-019-00407-8
- [15] S. Cmentowski, A. Krekhov, and J. Krüger. Outstanding: A Multi-Perspective Travel Approach for Virtual Reality Games. In Proceedings of the Annual Symposium on Computer-Human Interaction in Play, pp. 287–299. Acm, Barcelona Spain, Oct. 2019. doi: 10. 1145/3311350.3347183
- [16] R. Cools and A. L. Simeone. Investigating the Effect of Distractor Interactivity for Redirected Walking in Virtual Reality. In Symposium on Spatial User Interaction, Sui '19, article no. 4, 5 pages. Association for Computing Machinery, New York, NY, USA, 2019. doi: 10.1145/3357251.3357580

- [17] N. Coomer, S. Bullard, W. Clinton, and B. Williams-Sanders. Evaluating the Effects of Four VR Locomotion Methods: Joystick, Arm-Cycling, Point-Tugging, and Teleporting. In *Proceedings of the 15th ACM Symposium on Applied Perception*, Sap '18, article no. 7, 8 pages. Association for Computing Machinery, New York, NY, USA, 2018. doi: 10.1145/3225153.3225175
- [18] A. Drogemuller, A. Cunningham, J. Walsh, B. H. Thomas, M. Cordeil, and W. Ross. Examining virtual reality navigation techniques for 3D network visualisations. *Journal of Computer Languages*, 56:100937, Feb. 2020. doi: 10.1016/j.cola.2019.100937
- [19] N. Feld, N. Dubois, P. Bimberg, B. Weyers, and D. Zielasko. Dashing: Fun but Non-Ergonomic? Exploring Transition Effects in VR. In 2025 IEEE Conference on Virtual Reality and 3D User Interfaces Abstracts and Workshops (VRW), pp. 1–7, 2025. doi: 10. 1109/VRW66409.2025.00060
- [20] A. Field. Discovering statistics using IBM SPSS statistics. Sage publications limited, 4th ed., 2013.
- [21] P. M. Fitts. The Information Capacity of the Human Motor System in Controlling the Amplitude of Movement. *Journal of Experimental Psychology*, 47(6):381–391, 1954. doi: 10.1037/h0055392
- [22] P. M. Fitts and J. R. Peterson. Information Capacity of Discrete Motor Responses. *Journal of Experimental Psychology*, 67(2):103–112, 1964. Place: US Publisher: American Psychological Association. doi: 10.1037/h0045689
- [23] S. Freitag, B. Weyers, and T. W. Kuhlen. Interactive Exploration Assistance for Immersive Virtual Environments Based on Object Visibility and Viewpoint Quality. In 2018 IEEE Conference on Virtual Reality and 3D User Interfaces (VR), pp. 355–362, 2018. doi: 10. 1109/vr.2018.8447553
- [24] J. Frommel, S. Sonntag, and M. Weber. Effects of Controller-based Locomotion on Player Experience in a Virtual Reality Exploration Game. In *Proceedings of the 12th International Conference on the Foundations of Digital Games*, Fdg '17, article no. 30, 6 pages. Association for Computing Machinery, New York, NY, USA, 2017. doi: 10.1145/3102071.3102082
- [25] M. Funk, F. Müller, M. Fendrich, M. Shene, M. Kolvenbach, N. Dobbertin, S. Günther, and M. Mühlhäuser. Assessing the Accuracy of Point & Teleport Locomotion with Orientation Indication for Virtual Reality using Curved Trajectories. In *Proceedings of the* 2019 CHI Conference on Human Factors in Computing Systems, Chi '19, pp. 1–12. Association for Computing Machinery, New York, NY, USA, May 2019. doi: 10.1145/3290605.3300377
- [26] N. N. Griffin and E. Folmer. Out-of-body Locomotion: Vectionless Navigation with a Continuous Avatar Representation. In 25th ACM Symposium on Virtual Reality Software and Technology, pp. 1–8. Acm, Parramatta NSW Australia, Nov. 2019. doi: 10.1145/3359996 .3364243
- [27] N. N. Griffin, J. Liu, and E. Folmer. Evaluation of Handsbusy vs Handsfree Virtual Locomotion. In *Proceedings of the 2018 Annual Symposium on Computer-Human Interaction in Play*, pp. 211–219. Acm, Melbourne VIC Australia, Oct. 2018. doi: 10.1145/3242671.3242707
- [28] J. D. Hunter. Matplotlib: A 2D graphics environment. Computing in Science & Engineering, 9(3):90–95, 2007. doi: 10.1109/MCSE.2007 .55
- [29] jamovi. The jamovi project, 2024. (Version 2.6) [Computer Software]. Retrieved from https://www.jamovi.org.
- [30] P. Ke and K. Zhu. Larger Step Faster Speed: Investigating Gesture-Amplitude-based Locomotion in Place with Different Virtual Walking Speed in Virtual Reality. In 2021 IEEE Virtual Reality and 3D User Interfaces (VR), pp. 438–447, 2021. doi: 10.1109/vr50410.2021.00067
- [31] J. W. Kelly, A. G. Ostrander, A. F. Lim, L. A. Cherep, and S. B. Gilbert. Teleporting through virtual environments: Effects of path scale and environment scale on spatial updating. *IEEE Transactions on Visualization and Computer Graphics*, 26(5):1841–1850, May 2020. Conference Name: IEEE Transactions on Visualization and Computer Graphics. doi: 10.1109/tvcg.2020.2973051
- [32] R. Kopper, D. A. Bowman, M. G. Silva, and R. P. McMahan. A human motor behavior model for distal pointing tasks. *Interna*tional Journal of Human-Computer Studies, 68(10):603–615, 2010. doi: 10.1016/j.ijhcs.2010.05.001
- [33] E. Langbehn, P. Lubos, and F. Steinicke. Evaluation of Locomotion Techniques for Room-Scale VR: Joystick, Teleportation, and Redirected Walking. In *Proceedings of the Virtual Reality International Conference - Laval Virtual*, pp. 1–9. Acm, Laval France, Apr. 2018. doi: 10.1145/3234253.3234291

- [34] J. J. LaViola Jr, E. Kruijff, R. P. McMahan, D. Bowman, and I. P. Poupyrev. 3D User Interfaces: Theory and Practice. Addison-Wesley Professional, 2 ed., Mar. 2017.
- [35] J. Liu, H. Parekh, M. Al-Zayer, and E. Folmer. Increasing Walking in VR using Redirected Teleportation. In *Proceedings of the 31st Annual ACM Symposium on User Interface Software and Technology*, pp. 521–529. Acm, Berlin Germany, Oct. 2018. doi: 10.1145/3242587. 3242601
- [36] G. Loup and E. Loup-Escande. Effects of Travel Modes on Performances and User Comfort: A Comparison between ArmSwinger and Teleporting. *International Journal of Human–Computer Interaction*, 35(14):1270–1278, 2019. doi: 10.1080/10447318.2018.1519164
- [37] P. J. Líndal, K. R. Jóhannsdóttir, U. Kristjánsson, N. Lensing, A. Stühmeier, A. Wohlan, and H. H. Vilhjálmsson. Comparison of Teleportation and Fixed Track Driving in VR. In 2018 10th International Conference on Virtual Worlds and Games for Serious Applications (VS-Games), pp. 1–7, Sept. 2018. Issn: 2474-0489. doi: 10.1109/VS-Games.2018.8493414
- [38] E. S. Martinez, A. S. Wu, and R. P. McMahan. Research Trends in Virtual Reality Locomotion Techniques. In 2022 IEEE Conference on Virtual Reality and 3D User Interfaces (VR), pp. 270–280, 2022. doi: 10.1109/vr51125.2022.00046
- [39] Mighty Coconut. Walkabout Mini Golf VR, 2021. https://store.steampowered.com/app/1408230/Walkabout_Mini_Golf_VR/.
- [40] Othergate. Dungeons of Eternity, 2025. https://store.steampowered.com/app/3189340/Dungeons_of_Eternity/.
- [41] R. Paris, J. Klag, P. Rajan, L. Buck, T. P. McNamara, and B. Bo-denheimer. How Video Game Locomotion Methods Affect Navigation in Virtual Environments. In ACM Symposium on Applied Perception 2019, pp. 1–7. Acm, Barcelona Spain, Sept. 2019. doi: 10. 1145/3343036.3343131
- [42] A. Prithul, I. B. Adhanom, and E. Folmer. Teleportation in Virtual Reality; A Mini-Review. Frontiers in Virtual Reality, 2, 2021. doi: 10 .3389/frvir.2021.730792
- [43] K. Rahimi, C. Banigan, and E. D. Ragan. Scene Transitions and Teleportation in Virtual Reality and the Implications for Spatial Awareness and Sickness. *IEEE Transactions on Visualization and Computer Graphics*, 26(6):2273–2287, 2020. doi: 10.1109/tvcg.2018. 2884468
- [44] B. E. Riecke and D. Zielasko. Continuous vs. Discontinuous (Teleport) Locomotion in VR: How Implications can Provide both Benefits and Disadvantages. *Proc. of IEEE VR Abstracts and Work-shops*, pp. 373–374, 2021. doi: 10.1109/VRW52623.2021.00075
- [45] D. Rupp, T. Kuhlen, and T. Weissker. TENETvr: Comprehensible Temporal Teleportation in Time-Varying Virtual Environments. In 2023 IEEE International Symposium on Mixed and Augmented Reality (ISMAR), pp. 922–929, 2023. doi: 10.1109/ismar59233.2023.00108
- [46] D. Rupp, T. Weissker, M. Wölwer, T. Kuhlen, and D. Zielasko. [APK] How Far is Too Far? The Trade-Off between Selection Distance and Accuracy during Teleportation in Immersive Virtual Reality, Mar. 2025. doi: 10.5281/zenodo.15094088
- [47] D. Rupp, T. Weissker, M. Wölwer, T. Kuhlen, and D. Zielasko. [Supplemental Material] How Far is Too Far? The Trade-Off between Selection Distance and Accuracy during Teleportation in Immersive Virtual Reality, Apr. 2025. doi: 10.5281/zenodo. 15118258
- [48] A. Shahbaz Badr and R. De Amicis. An empirical evaluation of enhanced teleportation for navigating large urban immersive virtual environments. *Frontiers in Virtual Reality*, 3, 2023. doi: 10. 3389/frvir.2022.1075811
- [49] A. L. Simeone, N. Christian Nilsson, A. Zenner, M. Speicher, and F. Daiber. The Space Bender: Supporting Natural Walking via Overt Manipulation of the Virtual Environment. In 2020 IEEE Conference on Virtual Reality and 3D User Interfaces (VR), pp. 598– 606, 2020. doi: 10.1109/vr46266.2020.00082
- [50] S. R. Sindhupathiraja, A. K. M. A. Ullah, W. Delamare, and K. Hasan. Exploring Bi-Manual Teleportation in Virtual Reality. In 2024 IEEE Conference Virtual Reality and 3D User Interfaces (VR), pp. 754–764, 2024. doi: 10.1109/vr58804.2024.00095
- [51] R. W. Soukoreff and I. S. MacKenzie. Towards a standard for pointing device evaluation, perspectives on 27 years of Fitts' law research in HCI. *International Journal of Human-Computer Studies*, 61(6):751–789, 2004. Fitts' law 50 years later: applications and contributions from human-computer interaction. doi: 10.1016/j. ijhcs.2004.09.001
- [52] Valve. The Lab, 2016. https://store.steampowered.com/app/ 450390/The_Lab/.

- [53] S. Vlahović, M. Suznjevic, and L. S. Kapov. Subjective Assessment of Different Locomotion Techniques in Virtual Reality Environments. In 2018 Tenth International Conference on Quality of Multimedia Experience (QoMEX), pp. 1–3, May 2018. Issn: 2472-7814. doi: 10.1109/QoMEX.2018.8463433
- [54] T. Weissker, P. Bimberg, A. S. Gokhale, T. Kuhlen, and B. Froehlich. Gaining the High Ground: Teleportation to Mid-Air Targets in Immersive Virtual Environments. *IEEE Transactions on Visualization and Computer Graphics*, 29(5):2467–2477, 2023. doi: 10.1109/tvcg. 2023.3247114
- [55] T. Weissker, M. Franzgrote, and T. Kuhlen. Try This for Size: Multi-Scale Teleportation in Immersive Virtual Reality. *IEEE Transactions on Visualization and Computer Graphics*, 30(5):2298–2308, 2024. doi: 10.1109/tvcg.2024.3372043
- [56] T. Weissker, A. Kulik, and B. Froehlich. Multi-Ray Jumping: Comprehensible Group Navigation for Collocated Users in Immersive Virtual Reality. In 2019 IEEE Conference on Virtual Reality and 3D User Interfaces (VR), pp. 136–144, Mar. 2019. Issn: 2642-5254. doi: 10.1109/vr.2019.8797807
- [57] T. Weißker, A. Kunert, B. Fröhlich, and A. Kulik. Spatial Updating and Simulator Sickness During Steering and Jumping in Immersive Virtual Environments. In 2018 IEEE Conference on Virtual Reality and 3D User Interfaces (VR), pp. 97–104, 2018. doi: 10.1109/vr.2018.8446620
- [58] M. Wölwer, B. Weyers, and D. Zielasko. How Long Do I Want to Fade Away? The Duration of Fade-To-Black Transitions in Target-Based Discontinuous Travel (Teleportation). *Proc. of IEEE VR Ab*stracts and Workshops, pp. 817–818, 2024. doi: 10.1109/VRW62533. 2024.00205
- [59] S. Zhai, J. Accot, and R. Woltjer. Human Action Laws in Electronic Virtual Worlds: An Empirical Study of Path Steering Performance in VR. Presence, 13(2):113–127, 2004. doi: 10.1162/ 1054746041382393
- [60] D. Zielasko and T. Weissker. Stay Vigilant: The Threat of a Replication Crisis in VR Locomotion Research. In *Proceedings of the* 29th ACM Symposium on Virtual Reality Software and Technology, Vrst '23, article no. 39, 10 pages. Association for Computing Machinery, New York, NY, USA, 2023. doi: 10.1145/3611659.3615697

Daniel Rupp is a research associate at the Visual Computing Institute at RWTH Aachen in Germany. After graduating with a master's degree in computer science from RWTH Aachen University in 2022, he is now conducting research in the area of teleportation-based navigation, aiming to improve comprehensibility, efficiency, and navigational freedom to offer users a better way of exploring virtual environments without inducing motion sickness.



Tim Weissker is a senior scientist for virtual reality at the Visual Computing Institute of RWTH Aachen University where he is permanently appointed for conducting independent research in the broad area of virtual reality and 3D user interfaces. He leads the Virtual Reality Research Group at the institute, which conducts a diverse mixture of foundational as well as application-oriented research in the field. Tim's research interests include a large variety of topics on effective, efficient, and comfortable user interaction in

both single- and multi-user 3D virtual environments, all of which leverage the unique potential that virtual reality systems offer beyond the mere replication of real-world scenarios.



Matthias Wölwer is currently a master's student in computer science at Trier University. In 2023 he received his Bachelor of Science with a thesis on distance perception in virtual reality. He researched the impact of various discrete and delayed locomotion methods on the perception of virtual distances and surfaces. Since March 2024 he has been working as a research assistant at the Chair of Human-Computer Interaction at Trier University as part of the DFG research project "Put me There".



Torsten W. Kuhlen is a full professor and the head of the Virtual Reality & Immersive Visualization Group at RWTH Aachen University, Germany. His research interests include all areas of Virtual Reality with a focus on immersive data analysis in scientific and technical applications, the design and evaluation of 3D, multimodal human computer interfaces, and advanced navigation techniques in large virtual environments. In his career, Torsten Kuhlen has acquired and carried out numerous, mostly application-driven

and interdisciplinary research projects. Application domains comprise, among others, production technology, simulation science, medicine, and neuroscience. In Aachen, his group operates the aixCAVE, one of the largest VR installations worldwide. He has co-authored more than 250 peer-reviewed research papers and served as program chair, program committee member, and general chair for various renowned international conferences on Virtual Reality, Computer Graphics and Visualization.



Daniel Zielasko is an Associate Professor of Computer Science at the Technical University of Denmark (DTU). Previously, he was a postdoctoral researcher in the HCl group at Trier University, Germany. He earned his doctoral degree in 2020 at RWTH Aachen University, Germany, specializing in desk-centered VR. Collaborating across disciplines, he engaged with neuroscientists, psychologists, medical technicians, archaeologists, biologists, and geologists on various projects. Daniel integrates VR technologies

into everyday life, emphasizing professional workflows and entertainment. His interests include promoting environmental awareness, addressing cybersickness, and designing compelling and innovative 3D user interfaces to enhance immersive experiences.